ACS APPLIED MATERIALS & INTERFACES

RESEARCH ARTICLE

www.acsami.org

Effect of Side-Chain Structure of Rigid Polyimide Dispersant on Mechanical Properties of Single-Walled Carbon Nanotube/Cyanate Ester Composite

Wei Yuan,[†] Weifeng Li,[‡] Yuguang Mu,[‡] and Mary B. Chan-Park*[,†]

[†]School of Chemical and Biomedical Engineering, Nanyang Technological University, 62 Nanyang Drive, Singapore 637459, Singapore

[‡]School of Biological Sciences, Nanyang Technological University, 60 Nanyang Drive, Singapore 637551, Singapore

Supporting Information

ABSTRACT: Three kinds of polymer, polyimide without side-chain (PI), polyimide-*graft*-glyceryl 4-nonylphenyl ether (PI-GNE), and polyimide-*graft*-bisphenol A diglyceryl acrylate (PI-BDA), have been synthesized and used to disperse single-walled carbon nanotubes (SWNTs) and to improve the interfacial bonding between SWNTs and cyanate ester (CE) matrix. Visual observation, UV−vis−near−IR (UV−vis−NIR) spectra, and atomic force microscopy (AFM) images show that both PI-GNE and PI-BDA are highly effective at dispersing and debundling SWNTs in DMF, whereas PI is less effective. Interaction between SWNTs and PI, PI-GNE or PI-BDA was confirmed by computer simulation and Raman spectra. A series of CE-based composite films reinforced with different loadings of SWNTs, SWNTs/PI, SWNTs/PI-GNE and SWNTs/PI-BDA were prepared by solution casting. It was found that, because of the unique side-chain structure of PI-BDA, SWNTs/PI-BDA disperse better in CE matrix than do SWNTs/PI-GNE, SWNTs/PI, and SWNTs. As a result, SWNTs/PI-BDA/CE composites have the greatest improvement in mechanical properties of the materials tested. These results imply that the choice of side-chain on a dispersant is very important to the dispersion of SWNTs in matrix and the filler/matrix interfacial adhesion, which are two key requirements for achieving effective reinforcement.

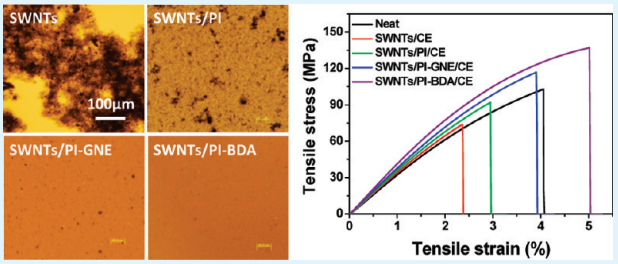

KEYWORDS: single-walled carbon nanotubes, cyanate ester, noncovalent, polyimide, side-chain, mechanical properties

INTRODUCTION

Carbon nanotubes (CNTs), which may be thought of as individual or nested concentric tubes formed by rolling two-dimensional sheets of graphite (graphene), are composed entirely of sp^2 hybridized carbon atoms.[1] This structure provides CNTs with excellent mechanical properties. For example, theoretical and experimental results show a tensile modulus of 640 GPa to 1 TPa[2] and a tensile strength of 150−180 GPa[3] for single-walled carbon nanotubes (SWNTs). The unique mechanical properties of CNTs make them ideal reinforcing fillers for polymer composites. However, the reinforcing efficiency of CNTs in composites depends strongly on the dispersion of CNTs in the polymer matrix and on the interfacial load transfer. One strategy used to improve the dispersion and interfacial bonding between CNTs and matrix is covalent functionalization with grafted small molecules[4−6] or polymeric chains.[7−9] However, covalent functionalization has the drawback that it disrupts the long-range π conjugation of the nanotubes, resulting in diminished mechanical properties.

In recent years, many polymers such as polythiophene,[10−12] poly(phenylene ethynylenes),[13,14] poly(phenylene vinylenes)[15] and polybenzimidazole[16] have been found to be good at dispersing CNTs by forming strong $\pi-\pi$ interactions with CNT side walls. Some of these polymer dispersants also have been successful for improving the mechanical properties of CNT/polymer composites.[12,14,16] Recently, Zou, Zhai and co-workers[11,17] showed that a conjugated block copolymer is a good dispersant for CNT dispersion/stabilization. The conjugated polymer block forms strong $\pi-\pi$ interactions with CNT walls while the non-conjugated polymer block located at the outer surface of the CNTs provides nanotubes with good solubility in solvents and polymer matrices. We hypothesize that a promising polymer dispersant for improving CNT dispersion and CNT/matrix interfacial bonding (and thus improving mechanical properties) would be a graft copolymer (or a block copolymer) in which the backbone (or the conjugated block) and the graft (or the nonconjugated block) were designed to favorably interact with CNTs and host polymer matrix, respectively. The usually tunable side-chain structure of a graft polymer dispersant should affect the mechanical properties of the resulting CNT/polymer composites.

Our previous study[18] showed that a graft copolymer, polyimide-*graft*-bisphenol A diglyceryl acrylate (PI-BDA), was very

Received: February 20, 2011
Accepted: April 28, 2011
Published: April 28, 2011

   dx.doi.org/10.1021/am2002229 | *ACS Appl. Mater. Interfaces* 2011, 3, 1702–1712

Scheme 1. Chemical Structures of (a) CE, (b) GAB, and (c) GNE

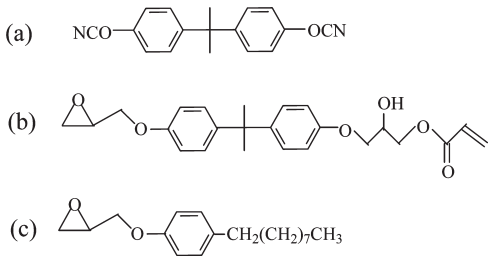

effective in dispersing SWNTs and improving the nanotube/matrix interfacial adhesion. This resulted in significantly improved mechanical properties of the resulting composites. In this study, in order to investigate the influence of the side-chain structure on the ability of polyimide graft to disperse SWNTs in matrix and to improve the SWNT/matrix interfacial bonding, polyimide backbone without side-chain (PI), and another graft polyimide with the PI backbone but grafted with glyceryl 4-nonylphenyl ether (GNE), PI-GNE, was synthesized. The dispersion of SWNTs, PI functionalized SWNTs (SWNTs/PI), PI-GNE functionalized SWNTs (SWNTs/PI-GNE) and PI-BDA functionalized SWNTs (SWNTs/PI-BDA) in DMF were characterized and compared. Furthermore, cyanate ester (CE) composite films with different contents of SWNTs, SWNTs/PI, SWNTs/PI-GNE and SWNTs/PI-BDA as reinforcement were prepared by solution casting. The nanotube dispersion in CE, nanotube/CE interfacial bonding, and mechanical properties of these four kinds of composites were investigated and compared. SWNTs/PI-BDA disperse best in CE matrix and show the greatest improvement in composite mechanical properties due to the unique side-chain structure of PI-BDA.

EXPERIMENTAL SECTION

Materials. Pristine CVD-grown SWNTs (purity ~90%, diameter 1−2 nm, length 5−30 μm) were obtained from Chengdu Research Institute of Organic Chemistry (China). They were purified with thermal oxidation (350 °C for 2 h in air) followed by acid treatment (refluxing in 6 M HCl for 12 h). Bisphenol A cyanate ester resin (CE, Scheme 1a) purchased from Shanghai Huifeng Technical & Business Co., Ltd. (Shanghai, China) with the trade name HF-1 was used as the resin. 3, 3′-dihydroxy-4, 4′-diaminobiphenyl (HAB, 97%) was purchased from Tokyo Chemical Industry. α-glycidyl-ω-acrylate terminated bisphenol A (GAB, Scheme 1b) with a molecular weight of 450 was supplied as Ebecryl 3605 from UCB chemicals (Malaysia). Glycidyl 4-nonylphenyl ether (GNE, technical grade, scheme 1c), 4-dimethylaminopyridine (DMAP, 99%) and all other chemicals were purchased from Sigma-Aldrich and used as received unless otherwise specified. *N*, *N*′-dimethylacetamide (DMAc) and dimethyl sulfoxide (DMSO) were distilled over calcium hydride and xylene over sodium wire under vacuum.

Synthesis of PI, PI-GNE and PI-BDA. PI and PI-BDA were synthesized via the methods described in our previous study.[18] In a typical procedure for synthesis of PI-GNE, PI (0.588 g, 1.20 mmol of repeat unit) was dissolved in 40 mL of dry DMSO at 60 °C in a 100 mL round-bottom flask equipped with a water condenser and an argon inlet/outlet. Then DMAP (0.293 g, 2.40 mmol) was added under argon protection. After the DMAP was completely dissolved, a solution of GNE (0.730 g, 2.64 mmol) in 20 mL of dry DMSO was added, and the resulting mixture was stirred at 100 °C for 48 h. The mixture was then poured into a large amount of methanol, and the precipitate was collected by filtration and washed successively with 0.2 M HCl solution, 5 wt % $NaHCO_3$ solution and DI water. Finally, the side-chain polyimide (PI-GNE) so obtained was vacuum-dried at 60 °C for 24 h. The yield was 0.778 g (62% yield). The weight-average molecular weight (M_w) and the polydispersity index (PDI) of the PI-GNE measured from GPC based on polystyrene standards were 5.5×10^4 g/mol and 1.35.

Preparation of Composite Films. To make composite films, various nanotube dispersions were first prepared. It has been demonstrated in our previous study[18] that 1:1 is the optimal mass ratio of PI-BDA to SWNTs for preparing nanotube dispersion, so in this study we also use the 1:1 mass ratio of dispersant to SWNTs. In a typical protocol used to prepare SWNTs/PI dispersion, 10 mg of SWNTs and 10 mg of PI were first added into 10 mL of DMF. Then the mixture was sonicated with a high-power tip sonicator (500 W, 35%, Vibra-Cell, Sonics) for 10 min followed by further sonication in a low-power sonic bath (S30H, Elma) for 30 min at 0 °C to produce a homogeneous SWNTs/PI dispersion (1 mg/mL SWNTs; the mass ratio of SWNTs to PI is 1:1). SWNTs/PI-GNE and SWNTs/PI-BDA dispersions were prepared by the same procedure by changing PI to PI-GNE or PI-BDA. Pristine SWNT suspension was prepared without the addition of polymeric dispersant.

Composite films with different contents of SWNTs were prepared by solution casting. A typical procedure for preparing SWNTs/PI/CE composite films was as follows: 0.1 g of CE that had been precured at 180 °C for 1 h was first dissolved in 0.1 mL of DMF. Then the CE solution was mixed with measured quantities of SWNTs/PI dispersion prepared as above. After sonication in a sonic bath for 10 min, the solution of SWNTs/PI/CE in DMF was cast onto a horizontal glass slide (26 mm ×76 mm × 1 mm). The slide was warmed on a hot plate at ~50 °C to slowly remove most of the DMF. Then the slide was transferred to a vacuum oven and dried under vacuum at 80, 100, and 120 °C for 2 h each. Finally, the films were cured in a convection oven. The curing cycle was 3 h at 180 °C, 2 h at 200 °C, and 2 h at 250 °C. After cooling to room temperature, the films were carefully peeled off the glass substrates. The thickness of the resulting film was about 40 μm, measured with a low torque digital micrometer. Neat CE films and CE composite films reinforced with SWNTs (SWNTs/CE), PI-GNE functionalized SWNTs (SWNTs/PI-GNE/CE), and PI-BDA functionalized SWNTs (SWNTs/PI-BDA/CE) were also prepared by a similar method.

Computer Simulation. We built a (10, 10) SWNT model (diameter ~1.4 nm) at length of 5 nm. For the all three polymers, PI, PI-GNE and PI-BDA, two repeating units were built. All-atom AMBER[19] general force field was used to represent SWNT, polymer, and DMF molecule. The aromatic carbon type with zero partial charge was assigned to carbon atoms of SWNT. The atomic charges of polymer and DMF were generated using RED software.[20] The validity of parameters of DMF was checked through calculating the density of pure DMF liquid, 0.92 g/cm^3, which is close to the experimental value of 0.95 g/cm^3. The simulation box was dodecahedral and contained one SWNT, one polymer and around 1500 DMF molecules. GROMACS[21] package with the help of Amb2gmx[22] conversion utility tool was used to perform the simulation. LINCS[23] protocol was employed to constrain all bonds involving hydrogen atoms in length. In all simulations, an integration step of 2 fs was used and nonbonded pair lists were updated every 10 fs. The system was coupled to an external heat bath with a relaxation time of 0.1 ps. Structure snapshots were output every 1 ps at 300 K for analysis. Particle mesh Ewald method[24] was used to treat electrostatic interactions with a cutoff of 9 Å. The van der Waals interactions were calculated by a cutoff of 12 Å. The binding free energy estimates were performed based on GB implicit solvent model[25] developed by Onufriev et al. provided by the sander module in AMBER 9.[19] The distance between SWNT and polymer at beginning was larger than 1 nm. For each SWNT-polymer system, three independent simulation

Scheme 2. Synthesis of PI-BDA and PI-GNE

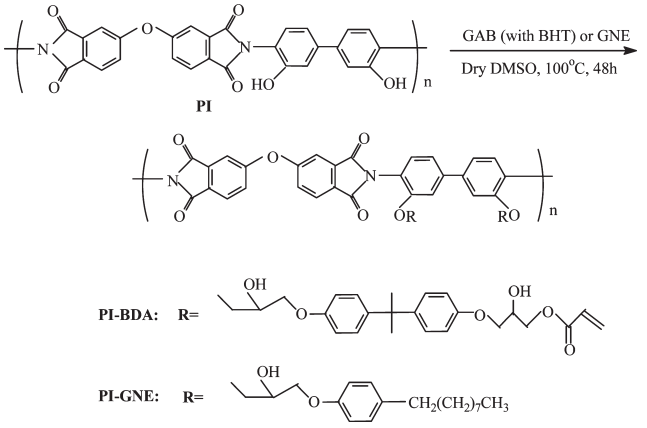

trajectories were conducted up to 60 ns. The last 30 ns trajectories were used for analysis.

Characterization. Fourier transform infrared (FT-IR) spectra were obtained on a Nicolet 5700 FT-IR instrument equipped with attenuated total reflectance (ATR) accessory. All measurements were made over the wavenumber range 400−4000 cm^{-1} at room temperature. Gel permeation chromatography (GPC) analyses were performed on a Shimadzu LC-20A Series GPC system equipped with a pump, a BC-PL gel mixed column (molecular weight limits ranging from 200−400,000 g/mol) and a RID-10A refractive index detector. DMF with 0.02 M LiBr was used as eluent at a flow rate of 1 mL/min at 60 °C. Analysis was based on calibration against polystyrene standards. Raman spectra of SWNTs and composite films were obtained with a Renishaw Ramanscope with HeNe laser at 633 nm excitation wavelength. UV−vis−near−IR (UV−vis−NIR) absorption spectra of nanotube dispersions were measured on a Varian Cary 5000 UV−vis−NIR spectrophotometer. Optical microscopy was carried out on an Olympus SZX12 microscope at a magnification of 144× . Atomic force microscopy (AFM) images were obtained using a MFP 3D microscope in ac mode. Nanotube dispersions were deposited onto clean silicon wafers by spin coating. Scanning electron microscopy (SEM) analysis was performed on a JEOL JSM-6700F Field-Emission Scanning Electron Microscope (FE-SEM) operating at 5 kV. The fracture surfaces of composites were coated with gold via sputtering in order to suppress surface charging effects. Tensile properties of composite films were measured with an Instron Model 5543 mechanical tester at room temperature. The films were cut into strips of 40 mm by 5 mm with varying thickness (~40 μm). A 100 N load cell and a cross head speed of 2.54 mm/min for effective sample length of 20 mm were used to do the testing. At least 5 measurements were made for each sample and the results were averaged.

RESULTS AND DISCUSSION

Synthesis of PI, PI-GNE, and PI-BDA. The synthesis and characterization of PI and PI-BDA has been discussed in our previous study.[18] Similarly to the synthesis of PI-BDA, the synthesis of PI-GNE was realized via reaction between the pendant hydroxyl groups on PI and epoxy groups on GNE with DMAP as catalyst. Scheme 2 shows the synthesis route of PI-BDA and PI-GNE.

Figure 1 shows the FTIR-ATR spectra of PI, GNE, and PI-GNE. The spectrum of GNE shows characteristic peaks of epoxy group at 917 cm^{-1}. The peaks at 2871, 2927, and 2957 cm^{-1} are identified as the C−H stretching mode of methyl and methylene

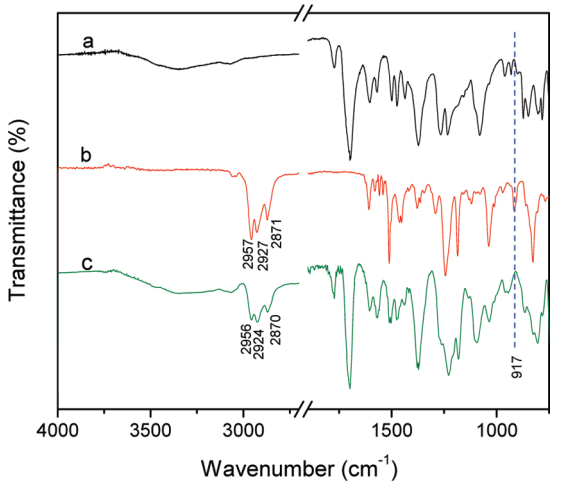

Figure 1. FTIR-ATR spectra of (a) PI, (b) GNE, and (c) PI-GNE.

groups. The spectrum of PI-GNE shows the characteristic peaks of its precursor PI, i.e., at 1772, 1699, and 1373 cm^{-1}, corresponding to the imide group, and at 1604, 1568, 1502, and 1475 cm^{-1}, corresponding to the aromatic C═C bands. After grafting the GNE side chain, new peaks at 2956, 2924, and 2870 cm^{-1} appear in the spectrum, which can be clearly assigned to the C−H stretches of $-CH_2$ and $-CH_3$ groups in the GNE side chain. A broad band at about 3700−3100 cm^{-1} in the spectrum of PI-GNE is attributed to the −OH group generated in the ring-opening reaction of epoxy groups (scheme 2). No characteristic peak of epoxy group (~ 917 cm^{-1}) appears in the spectrum. All these confirm successful grafting of GNE onto the PI backbone via reaction between −OH groups on PI and epoxy groups on GNE.

Dispersion of Nanotubes in DMF. Figure 2 compares the dispersion stability of SWNTs, SWNTs/PI, SWNTs/PI-GNE, and SWNTs/PI-BDA in DMF, at different standing times after sonication. Pristine SWNTs aggregated and settled within 10 days (Figure 2-2, vial A). SWNTs/PI partially aggregated but remained in suspension at 2 months (Figure 2-3, vial B). SWNTs modified with PI-GNE and PI-BDA were still well-dispersed and suspended at 2 months (Figure 2-3, vials C and D). These results indicate that the side chain grafted on the backbone of the PI, which imparts strongly repulsive forces to SWNTs/PI-GNE and -BDA via steric hindrance,[26] is very important to the long-term dispersion stability of the functionalized SWNTs in DMF. However, there was no obvious difference between the SWNTs/PI-GNE and SWNTs/PI-BDA dispersions.

The efficacy of PI, PI-GNE and PI-BDA at dispersing SWNTs was quantitatively compared using absorbance measurement and the Beer−Lambert law, which is defined as $A = \varepsilon lc$, where A is the absorbance at a fixed wavelength, ε is extinction coefficient, l is the light path length (1 cm for our cell), and c is the nanotube concentration.[27,28] The extinction coefficient (ε), which is strongly depended on naotube type, solvent type and wavelength of the measured absorbance, was determined in our previous study to be about 37.60 mL mg^{-1} cm^{-1} at 500 nm for our SWNTs in DMF.[18] Figure 3 shows the nanotube concentrations of SWNTs/PI, SWNTs/PI-GNE, and SWNTs/PI-BDA dispersions (mass ratio of SWNTs to polymer was fixed at 1:1) in different conditions, determined by measuring absorbance at 500 nm and the Beer−Lambert law. Immediately after sonication, all three of

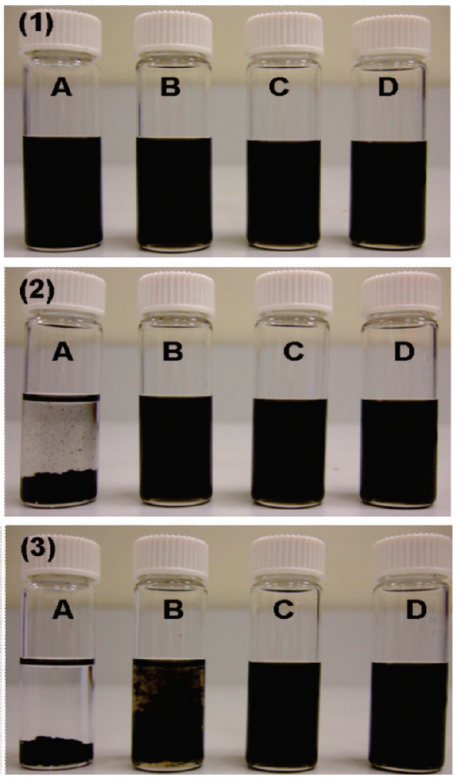

Figure 2. Visual observation of (A) SWNTs, (B) SWNTs/PI, (C) SWNTs/PI-GNE, and (D) SWNTs/PI-BDA in DMF at different standing times after sonication: (1) 0 min, (2) 10 days, and (3) 2 months.

the dispersions are homogeneous and have a suspended SWNT concentration of about 20 mg/L (the initial concentration we chose). After standing for 3 days, centrifugation at 6000 rpm for 1 h, and centrifugation at 14 00 rpm for 1 h, the SWNT concentrations of SWNTs/PI-GNE (19.8, 15.2, and 9.0 mg/L, respectively) and SWNTs/PI-BDA (20, 15.8, and 9.3 mg/L, respectively) are quite similar and are much higher than that of SWNTs/PI dispersion (18.7, 9.9, and 5.1 mg/L, respectively). These measurements are consistent with the results of visual observation.

The dispersions of SWNTs/PI, SWNTs/PI-GNE, and SWNTs/PI-BDA were also deposited onto silicon wafers and characterized by AFM (Figure 4). SWNTs were observed as large bundles with diameters of about 8−15 nm (Figure 4A). In SWNTs/PI (Figure 4B), the nanotube bundle diameters were reduced to be about 5 nm, and some individual tubes were also present. The measured heights of SWNTs/PI-GEN were in the range of 1−3 nm, indicating that they were dispersed as individual tubes as well as very small bundles (Figure 4C). SWNTs/PI-BDA (Figure 4D) are present similar as SWNTs/PI-GEN. Combined with the results of visual observation and UV−vis−NIR characterization, we conclude that PI-GNE and PI-BDA have similar efficacy at dispersing and debundling SWNTs in DMF.

To investigate the dispersion of SWNTs, SWNTs/PI, SWNTs/PI-GNE, and SWNTs/PI-BDA in CE matrix in DMF, we added 100 mg of partially prepolymerized CE (180 °C for 1 h) into 2 mL of nanotube/DMF dispersions (concentration fixed at 0.5 mg/mL, with dispersant to SWNT mass ratio of 1:1). In data not shown, after about 1 h, the SWNTs/PI/CE dispersion showed coagulation or agglomeration of the suspended nanotubes, while

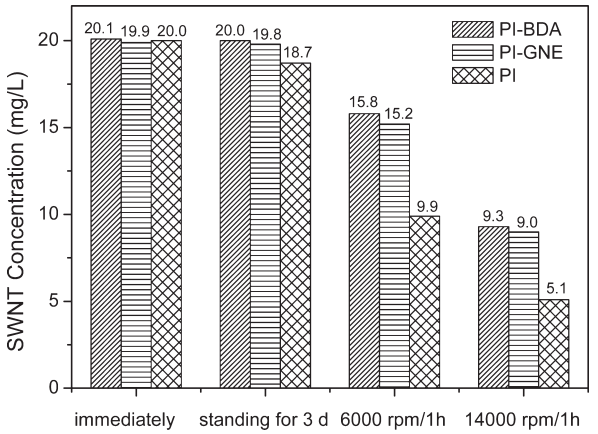

Figure 3. SWNT concentrations of SWNTs/PI, SWNTs/PI-GNE and SWNTs/PI-BDA dispersions (mass ratio of SWNTs to polymer is 1:1) in different conditions: immediately after sonication, standing for 3 days, centrifugation at 6000 rpm for 1 h, and centrifugation at 14 000 rpm for 1 h.

the SWNTs/PI-GNE/CE and SWNTs/PI-BDA/CE dispersions were very homogeneous. The quick precipitation of SWNTs/PI may be due to the poor stability of nanotubes dispersed with PI (Figure 2). After about 6 h, fine aggregates appeared in the SWNTs/PI-GNE/CE dispersion, while the PI-BDA functionalized nanotubes showed no visible evidence of gross aggregation after 24 h. The dramatic variation in behavior is further evidence that the precise nature of the side-chain is important in the design of polymer surfactants to disperse carbon nanotubes in a polymer (in this case, CE) solution. The structure of the PI-BDA side-chain is more similar to CE than is the PI-GNE side chain. This higher compatibility between the BDA side-chain and CE matrix results in higher efficiency of PI-BDA than PI-GNE in dispersing nanotubes in CE solution. Zou et al.[11] recently reported that a conjugated block polymer, poly(3-hexylthiophene)-*b*-polystyrene (P3HT-*b*-PS) is more efficient than homopolymer poly(3-hexylthiophene) (P3HT) in dispersing carbon nanotubes in polystyrene solution. They suggested that the PS segment, which has good solubility and miscibility with polystyrene matrix, is important for the high dispersion efficacy of P3HT-*b*-PS. For our PI-BDA surfactant, higher efficiency in dispersing CNTs in CE matrix can be expected if longer side-chains are grafted onto the PI backbone.

Computer Simulation of SWNT-Dispersant Systems in DMF. Molecular dynamics simulations were employed to study the interaction between SWNT and polymers PI, PI-GNE and PI-BDA in DMF. In the beginning of the simulations, the minimum distance between each polymer and the SWNT was more than 1.0 nm. For PI-GNE and PI-BDA, within a simulation time of 10 ns, the polymers formed close contacts with the SWNT, with the minimum distance between the polymer and SWNT being less than 0.3 nm. The contacts were very stable, no dissociation events happened in all simulations. However, in the case of PI, dissociation occurred frequently. During the total simulation time of 180 ns, the percentage of the SWNT-PI contacts formed was only 42%.

The strength of binding was estimated by calculating the binding energy which is defined as:

$$E_B = E_C{}^{GB} - (E_P{}^{GB} + E_{CNT}{}^{GB}) \quad (1)$$

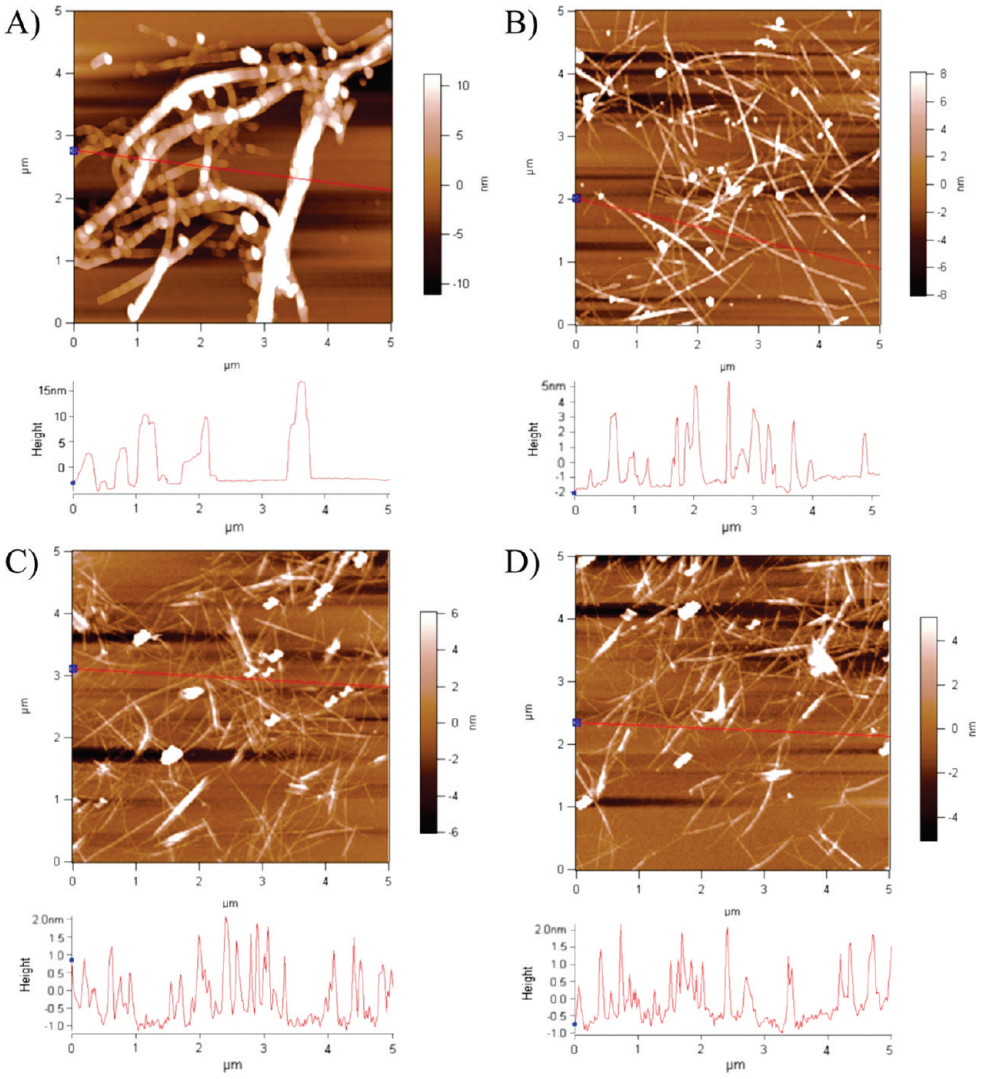

Figure 4. AFM images of (A) SWNTs, (B) SWNTs/PI, (C) SWNTs/PI-GNE, and (D) SWNTs/PI-BDA deposited on silicon wafers by spin coating.

where E_C^{GB}, E_P^{GB}, and E_{CNT}^{GB} are the energies of polymer−SWNT complex, polymer, and SWNT, respectively, based on the implicit generalized Born (GB) model. The binding energy of PI to SWNT is −12.9(±10.6) kcal/mol. In comparison, the binding energy of PI-GNE and PI-BDA to SWNT reaches −75.4(±16.7) kcal/mol and −78.3(±10.8) kcal/mol, respectively. The adding of side chains enhances the binding strength significantly. The binding patterns are illustrated by the complexes snapshots shown in Figure 5. It is evident that a small part of the PI, usually one or two rings, makes contacts with the SWNT surface, whereas the majority part of the molecule is solvated by the DMF solvent. The binding patterns are different for PI-GNE and PI-BDA, which adsorb well onto the SWNT surface. Clearly, the presence of side chains is essential to the intimate binding. The difference in the bonding strength and bonding pattern of PI, PI-GNE and PI-BDA to SWNT is consistent with the observation of dispersion state of SWNTs/dispersant in DMF.

Dispersion, Morphology, and Interfacial Bonding of Nanotubes in Composite Films. Optical micrographs can show the microscale state of the nanotube dispersion in the CE matrix. A representative optical micrograph of SWNTs/CE composite (Figure 6A) shows many aggregated clusters of SWNTs, suggesting nonuniform dispersion of SWNTs. The nanotube dispersion was improved for PI functionalized SWNTs, though some SWNT aggregates with sizes as large as 10 μm can be clearly seen (Figure 6B). In SWNTs/PI-GNE/CE composite (Figure 6C), dense aggregates are still apparent but the aggregate size is much smaller than that in the SWNTs/PI/CE composite, indicating much improved SWNT dispersion. By comparison, SWNTs/PI-BDA/CE composite show uniform dispersion of SWNTs throughout the matrix, and no obvious SWNT aggregates were observed (Figure 6D). It is interesting that SWNTs/PI-GNE and SWNTs/PI-BDA have similar dispersion in DMF, but the dispersion of SWNTs/PI-BDA in CE was much better than that of SWNTs/PI-GNE. In fact, the observation of a significant degree of SWNT aggregation in SWNTs/PI-GNE/CE composite is quite similar to the results reported by Delozier et al.,[29] who found that rigid polyimides grafted with alkyl side chains were good at dispersing SWNTs in DMAc but less effective in distributing SWNTs in polyimide composite films, especially at high CNT loading. The mechanical properties of their resultant SWNT/polyimide composites thus improved only very slightly. Comparing PI-BDA and PI-GNE, we attribute their different ability to disperse SWNTs in CE matrix to the

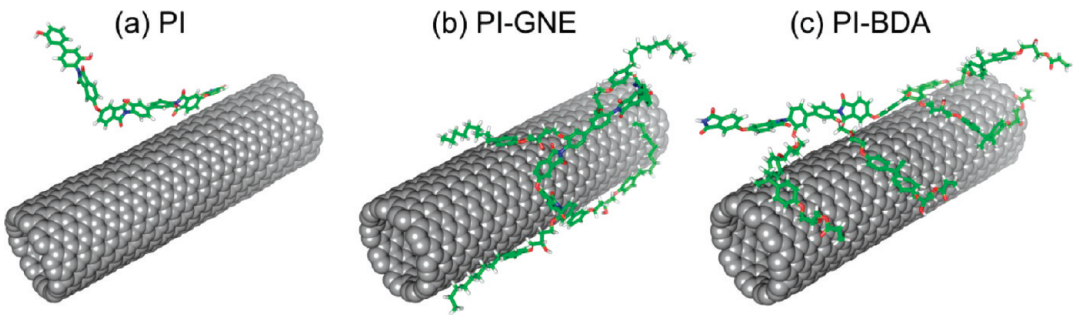

Figure 5. Snapshots of the complex of a (10, 10) SWNT and (a) PI, (b) PI-GNE, (c) PI-BDA. All structures are taken at the end of one trajectory (60 ns).

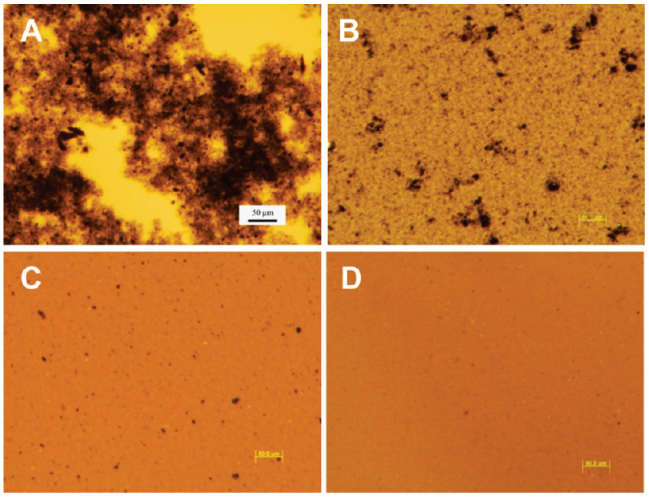

Figure 6. Optical micrographs of (A) SWNTs/CE, (B) SWNTs/PI/CE, (C) SWNTs/PI-GNE/CE, and (D) SWNTs/PI-BDA/CE composites with 1 wt % SWNT loading. Scale bars are 50 μm.

different structures of their side chains. The structure of PI-BDA side chain is more similar to that of CE monomer than is that of PI-GNE. This compatibility between the side-chain of PI-BDA and CE matrix reduces the likelihood of SWNT aggregation during film preparation. Because reduced aggregation and improved dispersion is expected to correlate with reinforcement efficacy of the filler, side-chain compatibility with the matrix is an important consideration in the design of effective SWNT-functionalizing materials.

The fracture surfaces of composite films after tensile testing were characterized with FE-SEM. In SWNTs(1 wt %)/CE nanocomposites, SWNTs are observed as agglomerated ropes divided by regions containing no SWNTs (Figure 7A1). Many nanotubes have been pulled out (Figure 7A2), leaving holes between nanotubes and CE matrix (indicated by arrows in Figure 7A3), which indicates weak interfacial bonding between SWNTs and CE matrix. PI functionalized SWNTs (Figure 7B1−B3) are also dispersed as aggregates in the CE matrix, and many of the tubes are found to be pulled out. However, the aggregate size is much smaller and the nanotube/matrix adhesion seems stronger when compared with SWNTs/CE. The fracture surface of SWNTs (1 wt %)/PI-GNE/CE composite films (Figure 7C1−C3) show much better SWNT dispersion in CE matrix compared to SWNTs/CE and SWNTs/PI/CE. But there is still some degree of SWNTs sliding and pulling out of the surface, although other SWNTs are found to have broken at the surface. Figure 7C3 clearly shows some big SWNT bundles pulled out (indicated by arrows). In SWNTs(1 wt %)/PI-BDA/CE composites (Figure 7D1−D3), SWNTs are homogeneously dispersed on the fracture surface and most of them are broken or only slightly pulled out from the surface. Figure 7D3 shows the diffuse character of the edges of the functionalized SWNTs, and some nanotubes with the exposed break end smaller than the end embedded in matrix (indicated by arrows). These suggest that the SWNTs are covered with a polymer shell and tightly embedded in the matrix, which would predict effective load transfer from matrix to SWNTs. All these fracture surface characteristics are in accordance with the mechanical properties of the corresponding composites, discussed below.

Raman spectroscopy has been used to study the interactions between carbon nanotubes and molecules based on the changes in the position of spectral features due to mechanical modes of the SWNTs.[30] Figure 8 shows the Raman spectra of SWNTs, and SWNTs/PI, SWNTs/CE, SWNTs/PI-GNE/CE, and SWNTs/PI-BDA/CE composite films. The peaks at around 1330 and 1590 cm^{-1} correspond to the defects- and disorder-induced modes (D band) and the in-plane E_{2g} zone-center mode (G band), respectively. As compared to pristine SWNTs, no significant increase in the D/G (defect/graphite) ratio was observed in the spectra of SWNTs/PI, SWNTs/PI-GNE and SWNTs/PI-BDA, indicating that few defects were introduced into the SWNTs and the nanotube length was well preserved. This is expected since the dispersants interact noncovalently with the SWNTs and the sonication applied for composite preparation was not very severe. The intact SWNT surfaces and long length contributes to the mechanical properties of the nanotube-reinforced composites. The G bands of SWNTs/CE (1588 cm^{-1}), SWNTs/PI/CE (1590 cm^{-1}), SWNTs/PI-GNE/CE (1591 cm^{-1}), and SWNTs/PI-BDA/CE (1592 cm^{-1}) composites were respectively upshifted by 3, 5, 6, and 7 cm^{-1} from the G band of neat SWNTs (1585 cm^{-1}). The 3 cm^{-1} upshift of G band in SWNTs/CE composites is due to the interaction between SWNTs and CE matrix which contains a large amount of triazine and benzene rings.[18,31] The 2−4 cm^{-1} higher upshifts in the SWNTs/PI/CE, SWNTs/PI-GNE/CE, and SWNTs/PI-BDA/CE composites compared to SWNTs/CE suggest that the electronic environment of the SWNT surfaces was changed by the polymeric dispersants. Aromatic compounds have been reported to interact with the graphitic sidewalls of CNTs via π-stacking.[31,32] The upshifts of G-band observed here clearly indicate the $\pi-\pi$ interaction between the SWNTs and the dispersants.[11,12] PI-BDA functionalized SWNTs were upshifted more than SWNTs/PI and SWNTs/PI-GNE, which may be attributed to their better dispersion resulting a greater degree of contact of SWNT sidewall with dispersant.

We believe that the stronger nanotube/matrix interfacial bonding in SWNTs/PI/CE, SWNTs/PI-GNE/CE and SWNTs/PI-BDA/CE

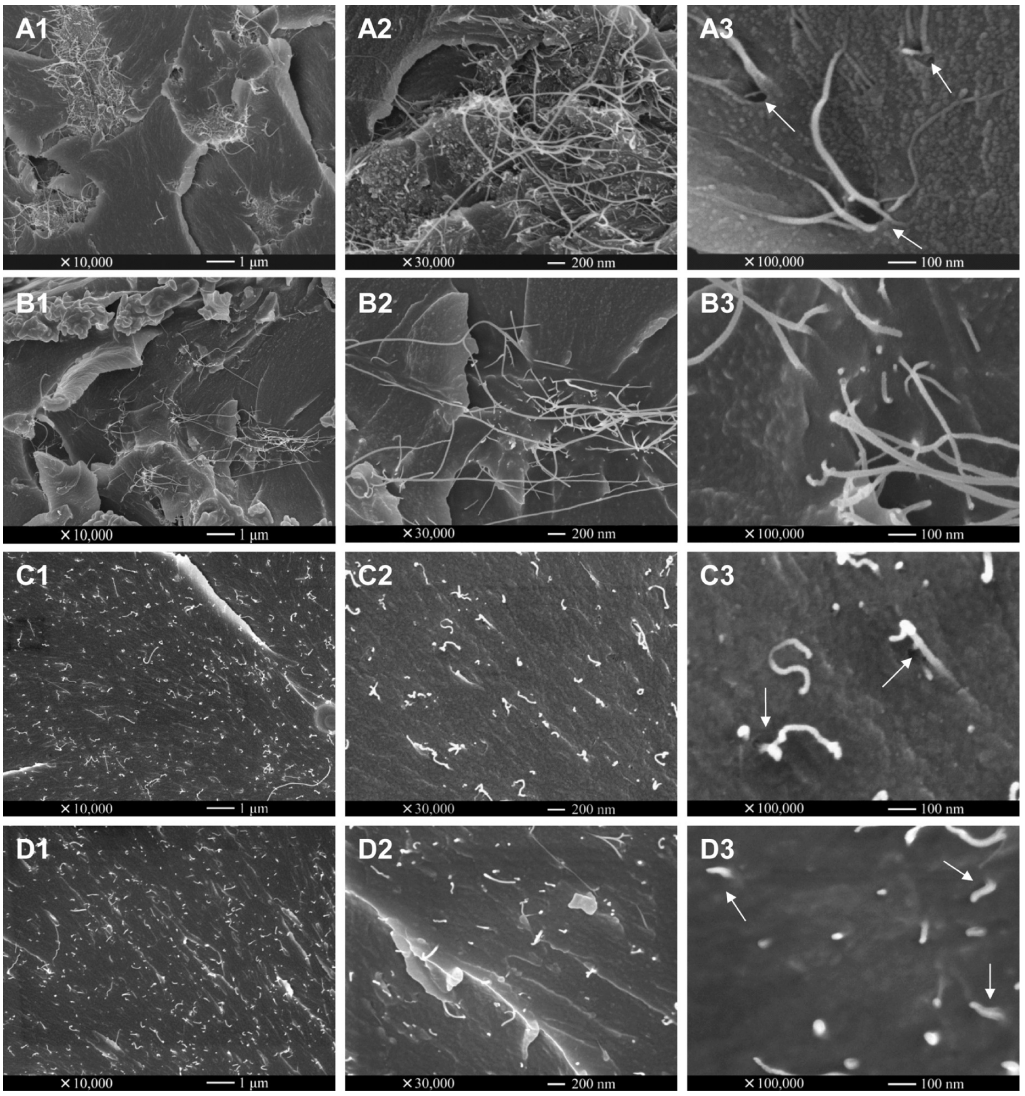

Figure 7. FE-SEM images of fracture surfaces of (A1−A3) SWNTs/CE, (B2−B3) SWNTs/PI/CE, (C1−C3) SWNTs/PI-GNE/CE, and (D1−D3) SWNTs/PI-BDA/CE composites. The SWNT loading in these composites is 1 wt %.

composites than in SWNTs/CE composite is due to polymeric dispersant adsorbed on nanotube surface, which not only improves the compatibility between nanotube and matrix but also reacts with CE matrix. The covalent reaction is realized via the reaction between −OH group on dispersants and −OCN group on CE matrix, which has been proved in our previous study.[18] The stronger interfacial bonding in SWNTs/PI-BDA/CE than in SWNTs/PI/CE and SWNTs/PI-GNE/CE can be attributed to the better dispersion of SWNTs/PI-BDA, which brings more dispersant-clad nanotube surfaces into contact with the surrounding CE matrix.

Mechanical Properties of Composite Films. The tensile properties, including Young's modulus (E), tensile strength (σ), elongation at break (ε), and toughness (T) of neat CE, SWNTs/CE, SWNTs/PI/CE, SWNTs/PI-GNE/CE and SWNTs/PI-BDA/CE composites with different SWNT loadings are summarized in Table 1 and Figure 9. Figure 9A shows representative tensile stress versus strain curves of neat CE and composites with SWNT loading of 1 wt %. The Young's modulus, tensile strength, elongation at break and toughness of the neat CE are 3.08 ± 0.14 GPa, 101.1 ± 6.0 MPa 4.0 ± 0.3% and 2.1 ± 0.2 MJ m^{-3}, respectively.

Figure 9B shows that for all four kinds of nanotubes, the Young's modulus (E) increases as the nanotube loading increases from 0 to 5 wt %, but the degree of improvement differs significantly for the different reinforcement materials. Compared with neat CE (E = 3.08 ± 0.14 GPa), the highest increase in E is about 7% (to 3.29 ± 0.11 GPa), 13% (to 3.48 ± 0.12 GPa), 24% (to 3.81 ± 0.15 GPa) and 41% (to 4.33 ± 0.14 GPa), respectively, for SWNTs/CE, SWNTs/PI/CE, SWNTs/PI-GNE/CE and SWNTs/PI-BDA/CE composites with 5 wt % of nanotubes. As shown in Figure 9C−E, SWNTs without dispersant lead to continuous decrease in σ, ε and T as the nanotube loading increases from 0 to 5 wt %. For SWNTs/PI/CE composite, a 0.2 wt % loading of SWNTs/PI gives the highest values of σ, ε and T, i.e., σ = 108.3 ± 7.7 MPa, ε = 4.3 ± 0.3%, and T = 2.4 ± 0.3 MJ m^{-3}, corresponding to 7%, 8% and 14% improvements over neat CE, respectively. Further increase of nanotube loading impairs tensile properties. With SWNTs/PI-GNE as reinforcement, the composites exhibit an increase in σ at low CNT loadings and a decrease at high CNT loadings. The SWNTs(1 wt %)/PI-GNE/CE composite has the highest strength of 122.3 ± 5.6 MPa,

corresponding to a 21% increase over neat CE. The ε and T increase initially at SWNT loading of 0.2 wt % but decrease continuously at higher SWNT loadings. The highest values of ε and T are 4.9 ± 0.2% and 3.1 ± 0.1 MJ m^{-3}, respectively, 23% and 48% above that of neat CE. The SWNTs/PI-DBA/CE composite films exhibit similar increasing trends with SWNT loading of σ, ε and T to those of SWNTs/PI-GNE/CE composite, but SWNTs/PI-BDA is more effective in mechanical reinforcement. The increase of σ continues up to 2 wt % of nanotube loading, the highest tensile strength at 2 wt % of nanotube is 148.1 ± 7.6 MPa, 46% above neat CE. The highest increase in ε is 43% (from 4.0 ± 0.3 to 5.7 ± 0.3%) achieved at SWNT loading of 0.5 wt %, whereas the highest increase in T is 90% (from 2.1 ± 0.2 to 4.0 ± 0.4 MJ m^{-3}) observed at SWNT loading of 1 wt %.

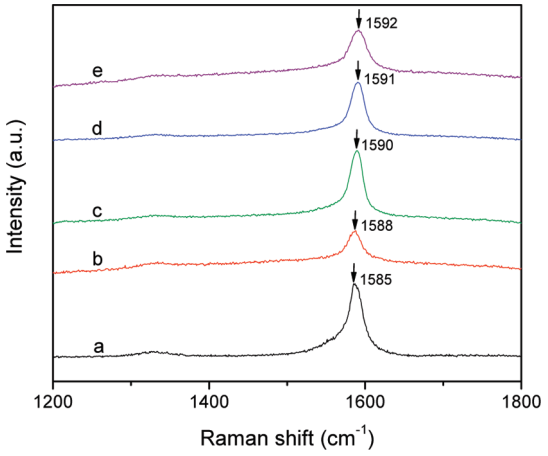

Figure 8. Raman spectra of (a) SWNTs, (b) SWNTs/CE, (c) SWNTs/PI/CE, (d) SWNTs/PI-GNE/CE, and (e) SWNTs/PI-BDA/CE composites. The SWNT loading is 5 wt %.

The tensile reinforcement efficacy of fillers can be quantitatively estimated from the variation rate of Young's modulus and tensile strength with weight fraction (dE/dW_{NT} and $d\sigma/dW_{NT}$).[18,33,34] Our SWNTs(1 wt %)/PI-BDA/CE composite possesses a dE/dW_{NT} value of 70 GPa and a $d\sigma/dW_{NT}$ value of 3540 MPa. These values compare favorably with results of CNT/thermosetting composites reported recently (dE/dW_{NT} and $d\sigma/dW_{NT}$ are 22−63 GPa and 140−2300 MPa, respectively),[4,6,35−38] which were calculated and listed in our previous study.[18] Our measurements on the tensile properties of dispersant/CE composites (without SWNTs) show that 1 or 5 wt % of dispersant has negligible effect on the tensile properties of the resulting CE composites (see the Supporting Information). So we conclude that the effect of these dispersant-functionalized SWNTs on tensile properties of CE can be mainly attributed to the SWNTs.

The poor reinforcement effect of SWNTs and SWNTs/PI is obviously due to the large SWNT aggregates and the weak interfacial adhesion between nanotubes and CE matrix, which have been discussed previously. The use of PI-GNE or PI-BDA functionalized SWNTs effectively enhances the mechanical properties of CE matrix. The superior reinforcement of CE matrix with SWNTs/PI-BDA as compared to that of SWNTs/PI-GNE is attributable to their better dispersion in CE matrix and stronger SWNT-CE interfacial interaction (and, consequently, more effective load transfer), as demonstrated by FE-SEM images of the fracture surface of composites (Figure 7) and Raman spectra (Figure 8). Our SWNTs/PI/CE, SWNTs/PI-GNE/CE, and SWNTs/PI-BDA/CE composites show increase of ε at relatively low CNT loadings, which is possibly due to the particular high aspect ratio and highly flexible elastic behavior of SWNTs during loading. In addition, the entangled SWNTs in matrix can be further stretched.[35] The increase of ε is helpful for improving the fracture toughness of composite, especially if the tensile modulus also increases. Both SWNTs/PI-GNE/CE and

Table 1. Mechanical Properties of Neat CE and CE Nanocomposites

sample	E (GPa)	σ (MPa)	ε (%)	T^a (MJ m^{-3})
neat CE	3.08 ± 0.14	101.1 ± 6.0	4.0 ± 0.3	2.1 ± 0.2
SWNTs(0.2 wt %)/CE	3.12 ± 0.09	90.3 ± 6.8	3.4 ± 0.3	1.6 ± 0.3
SWNTs(0.5 wt %)/CE	3.18 ± 0.17	75.1 ± 7.8	3.1 ± 0.2	1.3 ± 0.2
SWNTs(1 wt %)/CE	3.25 ± 0.11	66.2 ± 7.4	2.6 ± 0.5	0.9 ± 0.3
SWNTs(2 wt %)/CE	3.27 ± 0.13	48.7 ± 4.3	2.1 ± 0.2	0.6 ± 0.1
SWNTs(5 wt %)/CE	3.29 ± 0.11	40.6 ± 8.2	1.8 ± 0.4	0.4 ± 0.2
SWNTs(0.2 wt %)/PI/CE	3.18 ± 0.04	108.3 ± 7.7	4.3 ± 0.3	2.4 ± 0.3
SWNTs(0.5 wt %)/PI/CE	3.33 ± 0.16	93.5 ± 5.5	3.6 ± 0.5	1.9 ± 0.2
SWNTs(1 wt %)/PI/CE	3.37 ± 0.10	88.4 ± 9.1	3.2 ± 0.2	1.5 ± 0.1
SWNTs(2 wt %)/PI/CE	3.41 ± 0.23	73.6 ± 6.3	2.8 ± 0.5	1.2 ± 0.2
SWNTs(5 wt %)/PI/CE	3.48 ± 0.12	64.3 ± 8.9	2.2 ± 0.6	0.8 ± 0.2
SWNTs(0.2 wt %)/PI-GNE/CE	3.30 ± 0.13	117.8 ± 4.8	4.9 ± 0.2	3.1 ± 0.1
SWNTs(0.5 wt %)/PI-GNE/CE	3.40 ± 0.16	120.2 ± 6.3	4.4 ± 0.3	2.9 ± 0.3
SWNTs(1 wt %)/PI-GNE/CE	3.48 ± 0.05	122.3 ± 5.6	3.8 ± 0.2	2.6 ± 0.2
SWNTs(2 wt %)/PI-GNE/CE	3.67 ± 0.10	117.5 ± 5.2	3.6 ± 0.3	2.4 ± 0.2
SWNTs(5 wt %)/PI-GNE/CE	3.81 ± 0.15	110.7 ± 6.8	3.0 ± 0.6	1.9 ± 0.3
SWNTs(0.2 wt %)/PI-BDA/CE	3.35 ± 0.10	123.0 ± 5.7	5.2 ± 0.2	3.5 ± 0.2
SWNTs(0.5 wt %)/PI-BDA/CE	3.54 ± 0.06	128.2 ± 3.8	5.7 ± 0.3	3.9 ± 0.3
SWNTs(1 wt %)/PI-BDA/CE	3.78 ± 0.12	136.5 ± 5.4	5.2 ± 0.3	4.0 ± 0.4
SWNTs(2 wt %)/PI-BDA/CE	4.05 ± 0.07	148.1 ± 7.6	4.2 ± 0.4	3.6 ± 0.2
SWNTs(5 wt %)/PI-BDA/CE	4.33 ± 0.14	129.4 ± 8.6	3.6 ± 0.4	2.6 ± 0.3

[a] Calculated from the area under the stress−strain curve.

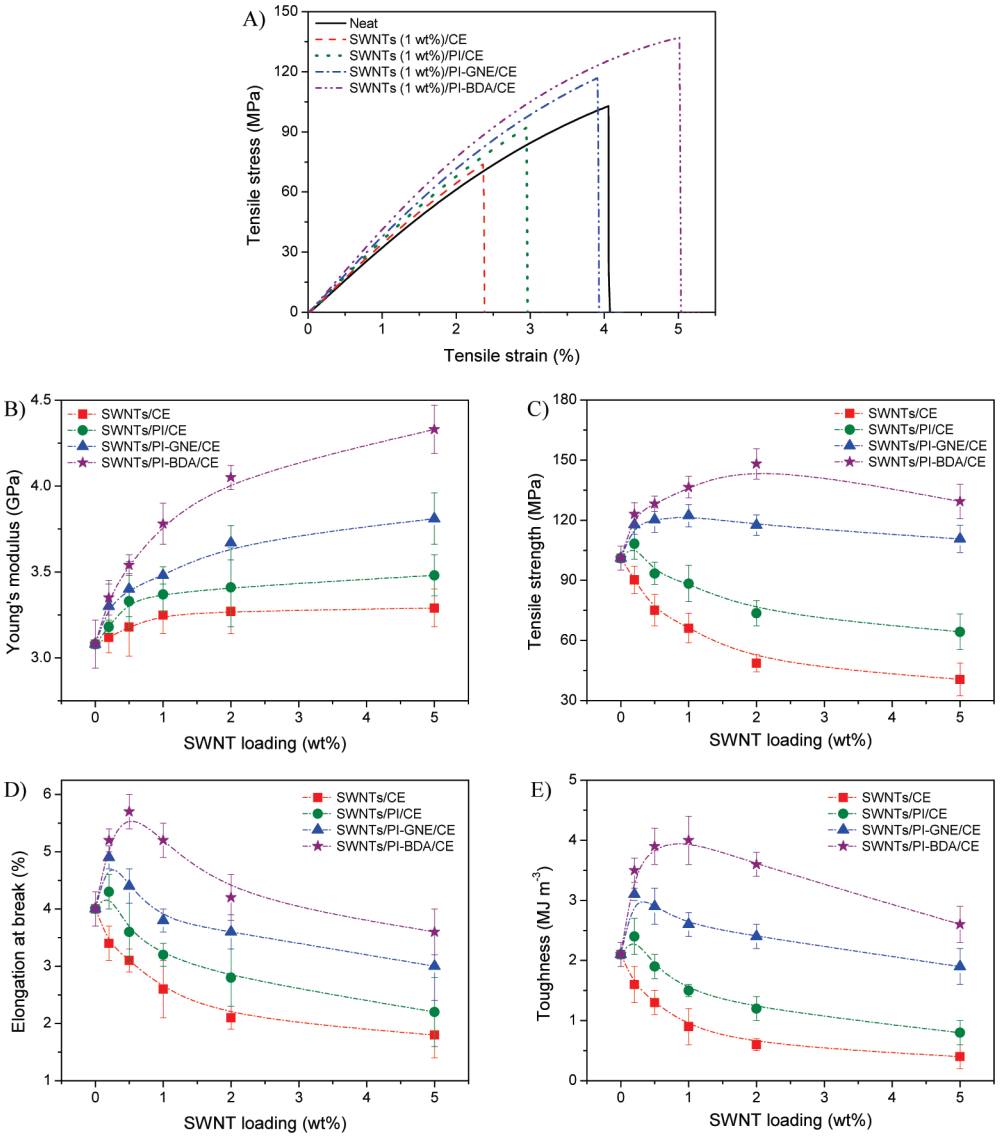

Figure 9. (A) Representative stress−strain curves of neat CE, SWNTs(1 wt %)/CE, SWNTs(1 wt %)/PI/CE, SWNTs(1 wt %)/PI-GNE/CE, and SWNTs(1 wt %)/PI-BDA/CE composites. Effect of SWNT content on (B) Young's modulus, (C) tensile strength, (D) elongation at break, and (E) toughness of SWNTs/CE, SWNTs/PI/CE, SWNTs/PI-GNE/CE, and SWNTs/PI- BDA/CE composites.

SWNTs/PI-BDA/CE composites show significantly increased toughness as compared with neat CE. This can be attributed to the homogeneous SWNT dispersion, which brings more dispersant-clad nanotube surface into contact with the CE matrix, and the strong nanotube/matrix interfacial bonding, both of which would resist the propagation of cracks during deformation, leading to increased fracture toughness.[39] Increased toughness for CE composite is very useful because the application of CE is sometimes limited by its brittle nature. Decrease in σ at high nanotube loadings is observed in our composites, which in fact is widely reported for other nanotube/polymer composites.[18,40,41] This may be due to poor wetting of CNTs at high nanotube loading, which leads to weak interfacial bonding. For our thermosetting matrix, another reason may be that CNTs may inadvertently affect the curing of thermosets and alter the network of cured matrix, especially near the interface between CNTs and matrix.[42]

We compare our experimental results with the values predicted from established models. Young's modulus data can be analyzed using the Halpin−Tsai model.[9,43,44] For randomly distributed SWNTs in a polymer matrix, the modified Halpin−Tsai equation is written as:

$$E_C = E_p\left[\frac{3}{8}\frac{1+2(l_f/d_f)\eta_L V_f}{1-\eta_L V_f}+\frac{5}{8}\frac{1+2\eta_T V_f}{1-\eta_T V_f}\right] \quad (2)$$

$$\eta_L = \frac{\left(\frac{E_f}{E_p}\right)-1}{\left(\frac{E_f}{E_p}\right)+2(l_f/d_f)} \quad (3)$$

$$\eta_T = \frac{\left(\frac{E_f}{E_p}\right)-1}{\left(\frac{E_f}{E_p}\right)+2} \quad (4)$$

dx.doi.org/10.1021/am2002229 |ACS Appl. Mater. Interfaces 2011, 3, 1702–1712

where E_C, E_f, and E_P are the tensile moduli of the composite, nanotube, and polymer matrix, respectively, l_f is the average SWNT length, d_f is the average SWNT or SWNT bundle diameter, and V_f is the SWNT volume fraction. The SWNT mass fractions can be converted into volume fraction using the relation

$$\frac{1}{V_f} = \left(\frac{\rho_f}{\rho_p}\right)\left(\frac{1-m_f}{m_f}\right) + 1 \qquad (5)$$

where V_f is the SWNT volume fraction, m_f is the SWNT mass fraction in polymer matrix and ρ_f and ρ_P are the densities of CNTs and polymer matrix, respectively. On the basis of the numerical values $\rho_f = 1.5$ g cm^{-3}, $\rho_P = 1.2$ g cm^{-3}, $l_f/d_f = 1000$, $E_P = 3.08$ GPa and $E_f = 640$ GPa,[44] the predicted moduli are 3.44 GPa, 3.97 GPa, 4.86 GPa, 6.66 GPa, and 12.10 GPa for composites with SWNT loadings of 0.2, 0.5, 1, 2, and 5 wt %, respectively. At low SWNT loading (i.e., 0.2 wt %), our experimental results (3.30 and 3.35 GPa for SWNTs(0.2 wt %)/PI-GNE/CE and SWNTs(0.2 wt %)/PI-BDA/CE composites, respectively) are very close to the predicted modulus (3.44 GPa), suggesting excellent SWNTs dispersion in the case of low nanotube loading. As the SWNT loading increases, the experimental modulus data diverge from the predicted values.

The tensile strength of CE composites reinforced with SWNTs can be predicted by a standard equation $\sigma_C = \sigma_f V_f + \sigma_m(1 - V_f)$,[45] where σ_C, σ_f, σ_P are the composite, the nanotube, and the polymer matrix strengths, respectively. V_f is the volume fraction of SWNTs. Using this equation with $\sigma_f = 30.0$ GPa,[46,47] $\sigma_m = 101.1$ MPa, the tensile strength of CE composites reinforced with SWNTs is calculated to be 148.9, 220.8, 340.8, 581.4, and 1309.1 MPa for CE composites with SWNT loadings of 0.2, 0.5, 1, 2, and 5 wt %, respectively. Our experimental results are lower than the predicted values, and the difference becomes larger as the SWNT loading increases.

Possible reasons for the lower experimental results than theoretical values may include the inevitable nanotube bundling, relatively weak nanotube/matrix interfacial bonding for noncovalently functionalized SWNTs, SWNT-induced impairment of the network of cured CE, some void defects in composites, and so on. We believe that better mechanical improvements can be achieved by optimizing these factors.

CONCLUSIONS

We have successfully synthesized three kinds of polymer, PI, PI-GNE and PI-BDA, all of which noncovalently react with SWNTs via $\pi-\pi$ interaction. PI-GNE and PI-BDA have similar high efficacy at dispersing SWNTs into individual tubes in DMF, while PI is less effective. Computer simulation and Raman spectra indicate the presence of $\pi-\pi$ interaction between SWNTs and polymeric dispersants. Carbon nanotube-reinforced CE composites were prepared by solution casting method, using SWNTs, PI, PI-GNE and PI-BDA functionalized SWNTs as fillers. SWNTs/PI-BDA better disperse in CE matrix and have stronger interfacial adhesion with CE than do SWNTs, SWNTs/PI and SWNTs/PI-GNE, which is due to the fact that the side chain BDA is more compatible with CE matrix and has stronger covalent bonding with CE. This makes SWNTs/PI-BDA the most effective at improving the mechanical properties of CE matrix. 2 wt% of SWNTs/PI-BDA increased the tensile modulus, strength and toughness of composite by 32, 47 and 71%, respectively. The experimental modulus and strength were lower than theoretical predicted values, especially at high nanotube loadings, which may be due to inevitable SWNT bundling, relatively weak SWNT-CE interfacial bonding and SWNT-induced impairment of the cured CE network. This study suggests that the side-chain structure of dispersant can greatly affect its ability to disperse SWNTs in polymer matrix and to improve the SWNT/polymer interfacial strength, both of which are important for effective mechanical reinforcement.

ASSOCIATED CONTENT

Supporting Information. Mechanical properties of neat CE and dispersant/CE composites. This material is available free of charge via the Internet at http://pubs.acs.org.

AUTHOR INFORMATION

Corresponding Author
*Phone: +65 6316 8938. E-mail: mbechan@ntu.edu.sg.

ACKNOWLEDGMENT

The authors acknowledge the financial support from the Defense & Science Technology Agency of Singapore (POD 0513240) and Singapore National Research Foundation through a Competitive Research Program grant (NRF-CRP2-2007-02).

REFERENCES

(1) Yang, M.; Koutsos, V.; Zaiser, M. *J. Phys. Chem. B* **2005**, *109*, 10009–10014.
(2) Uchida, T.; Kumar, S. *J. Appl. Polym. Sci.* **2005**, *98*, 985–989.
(3) De Heer Walt, A. *MRS Bull.* **2004**, *29*, 281–285.
(4) Zhu, J.; Kim, J.; Peng, H.; Margrave, J. L.; Khabashesku, V. N.; Barrera, E. V. *Nano Lett.* **2003**, *3*, 1107–1113.
(5) Pulikkathara, M. X.; Kuznetsov, O. V.; Khabashesku, V. N. *Chem. Mater.* **2008**, *20*, 2685–2695.
(6) Tseng, C. H.; Wang, C. C.; Chen, C. Y. *Chem. Mater.* **2007**, *19*, 308–315.
(7) Wang, M.; Pramoda, K. P.; Goh, S. H. *Polymer* **2005**, *46*, 11510–11516.
(8) Xie, L.; Xu, F.; Qiu, F.; Lu, H. B.; Yang, Y. L. *Macromolecules* **2007**, *40*, 3296–3305.
(9) Zhou, C. J.; Wang, S. F.; Zhang, Y.; Zhuang, Q. X.; Han, Z. W. *Polymer* **2008**, *49*, 2520–2530.
(10) Ikeda, A.; Nobusawa, K.; Hamano, T.; Kikuchi, J. *Org. Lett.* **2006**, *8*, 5489–5492.
(11) Zou, J. H.; Liu, L. W.; Chen, H.; Khondaker, S. I.; McCullough, R. D.; Huo, Q.; Zhai, L. *Adv. Mater.* **2008**, *20*, 2055–2060.
(12) Kim, K. H.; Jo, W. H. *Macromolecules* **2007**, *40*, 3708–3713.
(13) Chen, J.; Liu, H. Y.; Weimer, W. A.; Halls, M. D.; Waldeck, D. H.; Walker, G. C. *J. Am. Chem. Soc.* **2002**, *124*, 9034–9035.
(14) Chen, J.; Ramasubramaniam, R.; Xue, C.; Liu, H. *Adv. Funct. Mater.* **2006**, *16*, 114–119.
(15) Star, A.; Stoddart, J. F.; Steuerman, D.; Diehl, M.; Boukai, A.; Wong, E. W.; Yang, X.; Chung, S. W.; Choi, H.; Heath, J. R. *Angew. Chem., Int. Ed.* **2001**, *40*, 1721–1725.
(16) Okamoto, M.; Fujigaya, T.; Nakashima, N. *Adv. Funct. Mater.* **2008**, *18*, 1776–1782.
(17) Zou, J. H.; Khondaker, S. I.; Huo, Q.; Zhai, L. *Adv. Funct. Mater.* **2009**, *19*, 479–483.
(18) Yuan, W.; Feng, J.; Judeh, Z.; Dai, J.; Chan-Park, M. B. *Chem. Mater.* **2010**, *22*, 6542–6554.
(19) Case, D. A.; Darden, T. A.; Cheatham, T. E., III; Simmerling, C. L.; Wang, J.; Duke, R. E.; Luo, R.; Merz, K. M.; Pearlman, D. A.;

Crowley, M.; Walker, R. C.; Zhang, W.; Wang, B.; Hayik, S.; Roitberg, A.; Seabra, G.; Wong, K., F.; Paesani, F.; Wu, X.; Brozell, S.; Tsui, V.; Gohlke, H.; Yang, L.; Tan, C.; Mongan, J.; Hornak, V.; Cui, G.; Beroza, P.; Mathews, D. H.; Schafmeister, C.; S., R. W.; Kollman, P. A. *AMBER 9*; University of California: San Francisco, 2006.

(20) Cezard, C.; Vanquelef, E.; Pecher, J.; Sonnet, P.; Cieplak, P.; Derat, E.; Dupradeau, F. Y. *236th ACS National Meeting*, Philadelphia, PA, Aug 17−21, 2008; American Chemical Society: Washington, D.C., 2008.

(21) David Van Der, S.; Erik, L.; Berk, H.; Gerrit, G.; Alan, E. M.; Herman, J. C. B. *J. Comput. Chem.* **2005**, *26*, 1701–1718.

(22) Mobley, D. L.; Chodera, J. D.; Dill, K. A. *J. Chem. Phys.* **2006**, *125*, 084902–084916.

(23) Berk, H.; Henk, B.; Herman, J. C. B.; Johannes, G. E. M. F. *J. Comput. Chem.* **1997**, *18*, 1463–1472.

(24) Darden, T.; York, D.; Pedersen, L. *J. Chem. Phys.* **1993**, *98*, 10089–10092.

(25) Alexey, O.; Donald, B.; David, A. C. *Proteins: Struct., Funct., Bioinf.* **2004**, *55*, 383–394.

(26) Kim, K. K.; Yoon, S. M.; Choi, J. Y.; Lee, J.; Kim, B. K.; Kim, J. M.; Lee, J. H.; Paik, U.; Park, M. H.; Yang, C. W.; An, K. H.; Chung, Y. S.; Lee, Y. H. *Adv. Funct. Mater.* **2007**, *17*, 1775–1783.

(27) Bahr, J. L.; Mickelson, E. T.; Bronikowski, M. J.; Smalley, R. E.; Tour, J. M. *Chem. Commun.* **2001**, 193–194.

(28) Baskaran, D.; Mays, J. W.; Bratcher, M. S. *Chem. Mater.* **2005**, *17*, 3389–3397.

(29) Delozier, D. M.; Watson, K. A.; Smith, J. G.; Clancy, T. C.; Connell, J. W. *Macromolecules* **2006**, *39*, 1731–1739.

(30) Sinani, V. A.; Gheith, M. K.; Yaroslavov, A. A.; Rakhnyanskaya, A. A.; Sun, K.; Mamedov, A. A.; Wicksted, J. P.; Kotov, N. A. *J. Am. Chem. Soc.* **2005**, *127*, 3463–3472.

(31) Tournus, F.; Latil, S.; Heggie, M. I.; Charlier, J. C. *Phys. Rev. B* **2005**, *72*, 075431.

(32) Zhao, J. J.; Lu, J. P.; Han, J.; Yang, C. K. *Appl. Phys. Lett.* **2003**, *82*, 3746–3748.

(33) Che, J.; Yuan, W.; Jiang, G.; Dai, J.; Lim, S. Y.; Chan-Park, M. B. *Chem. Mater.* **2009**, *21*, 1471–1479.

(34) Yan, Y. H.; Zhao, S. A.; Cui, J.; Yang, S. B. *J. Polym. Sci., Part A: Polym. Chem.* **2009**, *47*, 6135–6144.

(35) Zhu, J.; Peng, H. Q.; Rodriguez-Macias, F.; Margrave, J. L.; Khabashesku, V. N.; Imam, A. M.; Lozano, K.; Barrera, E. V. *Adv. Funct. Mater.* **2004**, *14*, 643–648.

(36) Gojny, F. H.; Wichmann, M. H. G.; Kopke, U.; Fiedler, B.; Schulte, K. *Compos. Sci. Technol.* **2004**, *64*, 2363–2371.

(37) Song, Y. S.; Youn, J. R. *Carbon* **2005**, *43*, 1378–1385.

(38) Omidi, M.; Rokni, D. T. H.; Milani, A. S.; Seethaler, R. J.; Arasteh, R. *Carbon* **2010**, *48*, 3218–3228.

(39) Pan, Y.; Xu, Y.; An, L.; Lu, H.; Yang, Y.; Chen, W.; Nutt, S. *Macromolecules* **2008**, *41*, 9245–9258.

(40) Koval'chuk, A. A.; Shchegolikhin, A. N.; Shevchenko, V. G.; Nedorezova, P. M.; Klyamkina, A. N.; Aladyshev, A. M. *Macromolecules* **2008**, *41*, 3149–3156.

(41) Blond, D.; Barron, V.; Ruether, M.; Ryan, K. P.; Nicolosi, V.; Blau, W. J.; Coleman, J. N. *Adv. Funct. Mater.* **2006**, *16*, 1608–1614.

(42) Sun, L.; Warren, G. L.; O'Reilly, J. Y.; Everett, W. N.; Lee, S. M.; Davis, D.; Lagoudas, D.; Sue, H. J. *Carbon* **2008**, *46*, 320–328.

(43) Liu, L. Q.; Barber, A. H.; Nuriel, S.; Wagner, H. D. *Adv. Funct. Mater.* **2005**, *15*, 975–980.

(44) Zhang, X. F.; Liu, T.; Sreekumar, T. V.; Kumar, S.; Moore, V. C.; Hauge, R. H.; Smalley, R. E. *Nano Lett.* **2003**, *3*, 1285–1288.

(45) Gao, J. B.; Itkis, M. E.; Yu, A. P.; Bekyarova, E.; Zhao, B.; Haddon, R. C. *J. Am. Chem. Soc.* **2005**, *127*, 3847–3854.

(46) Che, J. F.; Chan-Park, M. B. *Adv. Funct. Mater.* **2008**, *18*, 888–897.

(47) Liu, L. Q.; Tasis, D.; Prato, M.; Wagner, H. D. *Adv. Mater.* **2007**, *19*, 1228–1233.